



Analyzing CW EPR Spectra of Nitroxide Labeled Macromolecules

Christian Altenbach¹ · David Budil²

Received: 12 July 2023 / Revised: 22 August 2023 / Accepted: 25 August 2023 /
Published online: 7 September 2023
© The Author(s) 2023

Abstract

Historically, the primary result of an EPR experiment is the CW EPR spectrum, typically displayed as the first derivative of the absorption spectrum as a function of the magnetic field. Beyond very qualitative assessments, the detailed analysis of an experimental EPR spectrum is a difficult inverse problem. Given a set of parameters and a model, it is easy to calculate a spectrum, but given an EPR spectrum, it is a challenge to decide on the correct model and find all defining parameters of interest. Programs to simulate and fit CW EPR spectra have been around for a long time. Except for a very well-defined model system, an experimental spectrum of a spin labeled protein is typically a mix of multiple states. This article focuses on the analysis of the CW spectrum in several stages of detail, from qualitative to detailed. The use of the EPR lineshape fitting program MultiComponent developed in the Hubbell lab is used to illustrate common approaches to extract information relevant to protein structure, function, dynamics, and thermodynamics.

1 Introduction

EPR spectroscopy of a spin label attached to a protein (or other biomolecule) can answer many questions about the structure, function, and dynamics of the protein under study and can fill in knowledge gaps where other methods fail. Systematic and detailed studies of spin labeled proteins were difficult before the advent of molecular genetics. This special issue is dedicated to Wayne Hubbell who had the vision to make EPR spectroscopy useful to the protein biochemist by developing all required parts through extensive collaborations with specialized labs covering many seemingly orthogonal disciplines. In the 1980s, a collaboration with Cyrus Levinthal [1] started exploring the possibility to use genetic engineering techniques to specifically

✉ Christian Altenbach
caltenba@ucla.edu

¹ Stein Eye Institute, UCLA, 100 Stein Plaza, Los Angeles, CA 90095, USA

² Northeastern University, Boston, MA 02115, USA

label a protein of interest at any desired position, thus introducing what is now called site-directed spin labeling (SDSL). In its infancy, this was a very hard problem with huge efforts required to get sufficient amounts of protein. These minute samples required better detection and in collaboration with Froncisz and Hyde, the loop-gap resonator made the acquisition of EPR spectra feasible for these systems [2]. Working at the Jules Stein Eye institute, the light receptor of the eye, rhodopsin, was of course the most obvious target of interest, but it took many years by the Khorana lab at MIT to produce usable amounts. Until rhodopsin could be studied, bacteriorhodopsin was a more approachable model analog and was used to develop and hone the EPR techniques with great success [3–5], putting all the tools in place to systematically study the structure and function of a transmembrane protein. Once rhodopsin was feasible, nitroxide scanning of the entire cytoplasmic face of rhodopsin was not only able to determine global structure in the dark state, but the qualitative mobility changes as a function of light activation pinpointed hotspots of helix movement by mapping increases and decreases in mobility for each site [6, 7]. While these results were necessarily very qualitative, they were later confirmed and quantified by distance measurement using EPR DEER [8] and crystallography [9–12]

The advent of site directed spin labeling has opened the floodgates to produce an ever-growing collection of spin labeled proteins and their concomitant EPR spectra. Unlike model systems such as the spectrum of a small, approximately spherical nitroxide as a function of temperature and viscosity, these spectra are typically impossible to describe with a simple model. Most of the time, the interpretation of EPR spectra has remained quite qualitative. A deep understanding of the factors determining the lineshape required comparisons with crystal structures of spin labeled model systems [13, 14] and molecular dynamics computations [15–18].

EPR spectra of a nitroxide spin label attached to a biomolecule can be very complicated. They depend on local bond rotations, the geometric restrictions imposed by the surrounding protein structure, as well as properties of the environment, such as solvent polarity. The protein itself can be in an equilibrium of multiple states in slow exchange (active, inactive, unfolded, etc.) and each state will typically result in a unique EPR spectrum. Even the nitroxide side chain can be in multiple conformations [14]. The resulting spectrum will be a weighted sum of all the component spectra. This article focuses mostly on spin labeled proteins, but similar work has been done on other types of macromolecules such as spin labeled RNA and DNA [19–23].

There is a deep chasm between the interests of a typical protein biochemist working in the trenches and the theoretical works to mathematically model an EPR line shape based on detailed models with a huge set of parameters that describe the magnetic characteristics, motional rate, geometric restrictions, and environment of the spin label. Extensive collaborations from both sides were of course ever-present [24]. Although there are a few different theoretical approaches to calculating the EPR spectrum of nitroxides undergoing slow motion (surveyed in reference [25]) the one most suited to lineshape fitting is the stochastic Liouville equation approach developed by Freed and coworkers. The high computational efficiency of this method enables convenient, and rapid real-time iterative fitting algorithms, at the

expense of approximating some of the dynamic details by describing the motion in terms of a diffusion model [26].

A computer program for a single spectrum lineshape calculation was first distributed by Schneider and Freed [27] in the form of a floppy disk with Fortran source code for the EPRL program. Several nonlinear least-squares programs based on this code or subsequent developments of the code have also been distributed. The first of these programs was a command-line driven program for Windows-based systems described by Budil et al. [28] which introduced several conventions that have been widely adapted by subsequent fitting programs. These included (1) a graphical window to provide visual feedback to enable user control of the procedure, (2) varying dynamic variables on a logarithmic scale, (3) allowing tensor parameters to be varied in cartesian or spherical form, (4) multicomponent fitting with automated shifting and scaling, and (5) basic parameter error analysis. More recently, an expanded version of the slow-motion calculation engine with several additional capabilities including lineshape fitting was added to the EasySpin suite of programs originally developed by Stoll in the laboratory of Schweiger [29] and later extended and distributed by the Stoll group [30, 31] in MATLAB. EasySpin also utilizes command-line entry with a graphical interface for the fitting procedure. Most recently, Bruker has added the capability of fitting slow-motion EPR lineshapes to its SpinFit software.

Around 2006, the first version of a standalone program with a fully graphical user interface was released to allow fitting of EPR spectra that contain up to four unique spectral components as often encountered experimentally: MultiComponent by Christian Altenbach from the lab of Wayne L. Hubbell. It facilitated the analysis of experimental spectra in significantly more detail with an easy-to-use graphical user interface and highly optimized code. One of the major strengths of MultiComponent is the calculation and fitting speed, especially for the case of microscopic order with macroscopic disorder (MOMD), which is often applicable for protein work.

2 Classes of SDSL-EPR Experiments

EPR spectroscopy can study proteins in the native environment at room temperature while avoiding the limitations of other structural methods such as NMR, which requires large amounts of protein and cannot handle large membrane proteins, or X-ray crystallography, which requires crystallization of the protein that may lead to artifacts that trap the protein in a physiologically irrelevant conformational substate [32].

It all starts with a specifically labeled protein. Using site directed spin labeling (SDSL) [33], a single side-chain (most often a genetically introduced cysteine) is replaced with a suitable EPR active stable free radical and the spectrum recorded. Classically, the radical is a nitroxide analog, modified to provide the desired chemical reactivity for attachment. Other types of labels are possible including triarylmethyl radicals [34] and complexes of paramagnetic ions [35–37]; however, these labels are primarily designed for distance measurements, whereas the

smaller nitroxide moiety is most suitable for measuring dynamics, which is the focus of this article.

The most popular nitroxide spin label, R1, has been extensively studied and the dynamic behavior when attached to a protein (Fig. 1) is well understood from comparisons with X-ray structures [13] and extensive molecular modeling. For helical surface sites, the motion is predominantly limited to rotations of only two bonds (X4–X5) [38, 39]. Similarly, the resulting line shapes on other secondary structures (mobile loop, internal sites, beta sheet surface) have been investigated as a function of neighboring side chains and partial contacts with other parts of the protein [40–43]. Beyond R1, many other nitroxide spin labels have been tailored to answer specific questions. In particular, the lab of Kalman Hideg and Tamás Kálai [43–49] has been instrumental in generating any imaginable nitroxide derivative for this purpose [50]. For example, a bifunctional (RX) nitroxide can limit side chain motion to better report dynamics of the protein backbone [13, 32, 38, 51, 52].

The interpretation and desired details strongly depend on the needs of the investigator and the experiment must be tailored accordingly. For some experiments, it is sufficient to have a single spin labeled protein engineered to be sensitive to the features of interest, but it is recommended to try multiple sites for a conclusive picture. Accessibility studies and distance measurements can round out the picture but will not be discussed here [32].

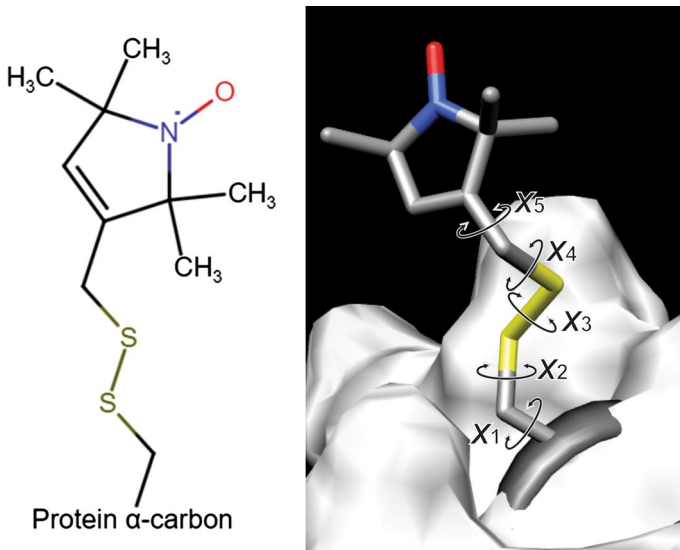


Fig. 1 The structure of the R1 nitroxide side chain and a 3D representation on a protein surface. From all the possible bond rotations shown (χ_1 – χ_5), typically only χ_4 and χ_5 contribute to the local averaging when R1 is on a helical surface site

2.1 Nitroxide Scanning

In a nitroxide scanning experiment the spin labeling is placed successively over a sequence of adjacent sites in the region of interest. Here it might be sufficient to classify the spectrum along an arbitrary scale from “mobile” to “immobile”. Regular oscillations of the mobility can be used directly to determine secondary structure and the values are self-calibrating because we just look at relative mobilities compared to neighboring sites. For example, while there is a strong background mobility gradient in helix 6 of rhodopsin [6], the relative oscillations still report the periodicity of a helical structure.

Having obtained the structural features of the inactive state, the experiment can be repeated in the active state and relative changes at each site give direct information on the nature, localization, and direction of the activation mechanism. The term activation is used here very generically and encompasses any change in state caused by external changes in condition, see below.

For simple structural studies, analyzing the exact EPR lineshape is not very important. However, the resulting large collection of such spectra is useful to test if the mathematical models are sufficient to explain these lineshapes and can provide feedback to the theoretical work and extension of the theory. Even if the lineshape is complicated, simple measurements can be obtained by fitting. Ideally, the resulting best fit can be reduced to very few descriptive, but interesting parameters that can then be graphed as a function of position.

2.2 Equilibrium Studies

While a single EPR spectrum depends on a huge number of parameters and settings, typically only a few are of interest to the protein chemist. For example, if the protein is in an equilibrium of two or more states, the most interesting are the relative populations [53, 54]. Here we simply want to determine relative amounts of each component as a function of state and it is more important to get a good fit for each unique spectral component, while the magnetic and dynamic properties are of secondary interest only. That equilibrium can often be shifted as a function of external conditions such as temperature, pressure [54, 55], denaturant concentration, ligand concentration, activation by light [56–59] or activation by ligand [60–62]. An analysis of the relative populations allows determination of thermodynamic parameters that have nothing directly to do with EPR spectroscopy or any deep understanding of the EPR line shape. Many environmental modifiers may change the detailed spectral shape of each component and thus the set of results cannot be described as a simple linear combination of the same spectral components differing only in relative amounts. This also precludes model-free techniques such as SVD or PCA to directly analyze the data. Each composite spectrum must be fitted to a model to obtain the relative amplitudes along the state variable. The investigator might be confronted with the two spectra shown in Fig. 2. To measure the relative amounts of the two interesting components A and B, a fit to four components is required.

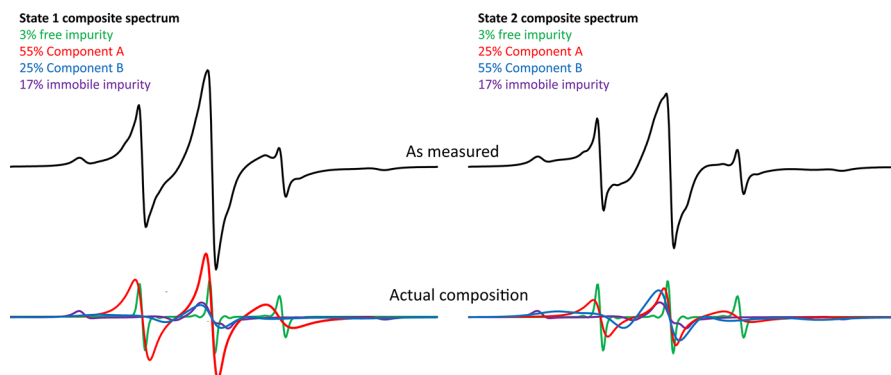


Fig. 2 Simulated multicomponent spectra for two states of the same protein. The condition changes the equilibrium between the two interesting states A and B while the impurities are invariant. In a typical experiment the shapes of all components are slightly state dependent. Only the black spectra can be measured, but a full MultiComponent analysis is required to determine ratio of A and B in the two samples to deduce thermodynamic parameters. Because minute differences are amplified in the first derivative display, a good approximate fit is typically sufficient to determine relative amounts quite accurately

There are several techniques to obtain EPR spectra that do not depend on classic field modulation detection and can give complementary information while avoiding modulation artifacts; examples include multiquantum [63], rapid scan [64], spin echo detected [65], and saturation recovery (SR) detected [66] signals. SR detection is an interesting case, because multiple exponentials at each field position can be used to extrapolate component spectra directly. The interpretation of the lineshape is typically independent of the acquisition technique. Some methods give the absorption spectrum instead of the first derivative, but all results are suitable to be analyzed with MultiComponent.

3 The Origin of the EPR Lineshape

In a nutshell, for any given static orientation of the nitroxide group with respect to the magnetic field, the EPR spectrum is composed of three lines due to the presence of the nearby ^{14}N nuclear spin. The field position of the center line, B depends on the effective electronic g -value at that orientation g_{eff} and the spectrometer frequency ν via the resonance condition $B = h\nu/g_{\text{eff}}\beta$ where h is Planck's constant and β is the Bohr magneton, and the splitting between each pair is the effective ^{14}N hyperfine interaction at that orientation. The orientation dependence of the spectrum is strong as shown in Fig. 3. Integrating over all orientations in space results in the rigid limit (powder) spectrum. If the spin label is allowed to rotate with a rate that is very fast compared to the microwave frequency, these tensors collapse and all we get is a spectrum with three sharp lines with the position and splitting given by the average tensor values (often labeled g_0 , A_0 , but named g_1 , A_1 in the program for historical reasons). In the two extreme cases shown, *complete averaging* or *rigid limit*, the spectrum is easy to compute from first principles. However, a nitroxide attached to a macromolecule will fall in-between

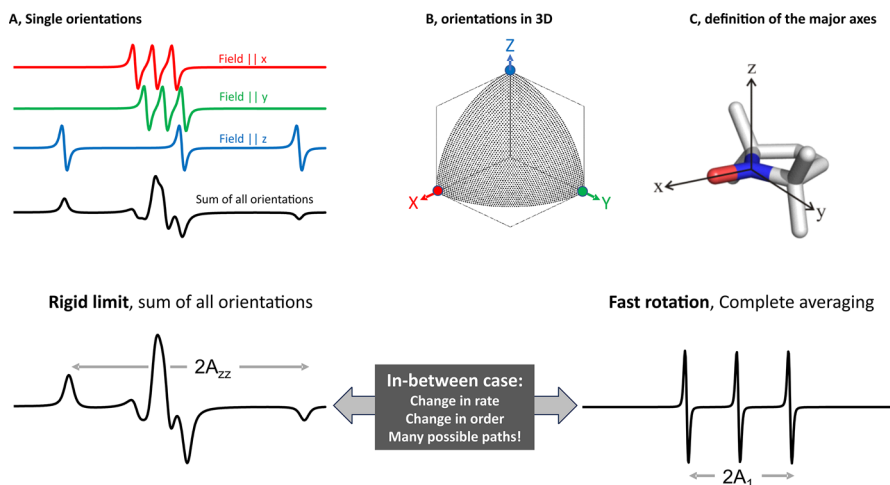
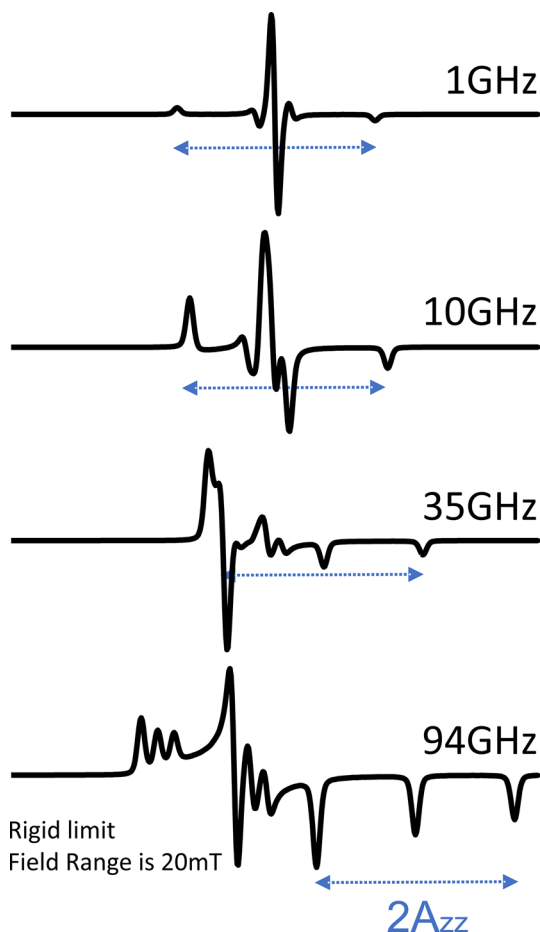


Fig. 3 The origin of the nitroxide EPR lineshape. Due to the nuclear spin of the nearby ^{14}N , there are always three lines, but their position and splitting strongly depend on the orientation of the molecule with the magnetic field. Three examples are shown for orientation along the three major axes at X band. Summing up all possible orientations (one octant is sufficient because of symmetries) results in the rigid limit powder spectrum. In the presence of fast rotation around all axes, the asymmetry averages out and three sharp lines are observed. There are many possible paths between these two extreme cases (see text for details)

these extremes and there are many possible paths to go from “rigid limit” to “fast isotropic motion” and the intermediary spectra can differ dramatically depending on the path taken. Tumbling can differ in rate and there will be geometric restrictions that, due to allowed bond rotation and the surrounding protein structure, can restrict averaging to a subset of all possible angles, while the protein itself will still have all possible orientations. Both rate and order can be anisotropic for a great variety of possibilities. The real system can be approximated assuming certain symmetries and simplifications. The rotational rate is also a tensor and can be non-isotropic (axial, rhombic). The rotational diffusion tensor \mathbf{R} can have arbitrary orientation relative to the magnetic tensors ($[A]$, $[g]$) but is locked to the nitroxide group. Order can be approximated with potentials expressed as spherical harmonics. Simulating such a spectrum requires a model, and many models are implemented in the software discussed below.

Note that there is also a strong frequency dependence: the g tensor scales directly with the microwave frequency while the A tensor is frequency independent. Figure 4 shows how the g tensor starts dominating at higher frequencies. Higher frequencies increase the width of the spectral features dictated by the g anisotropy, thus requiring faster rotational diffusion for effective averaging.

Fig. 4 Rigid limit spectra simulated for various microwave frequencies. Field Range is 20 mT, (or 200 Gauss). The center fields are approximately 36 mT, 360 mT, 1250 mT, or 3350 mT, respectively



4 Interpretation of an EPR Spectrum Using MultiComponent

While coarse features of an EPR spectrum can be gleaned without resorting to simulation and fitting, an easy to use and menu driven graphical tool to analyze EPR lineshapes is useful. It should expose all available features to the expert but should also be easy to use by researchers outside the field of EPR spectroscopy and as a learning tool for students. MultiComponent is a turnkey standalone program for Microsoft Windows that does not require secondary skills such as knowledge of the MATLAB programming environment. All parameters and settings have reasonable default values. User feedback is instantaneous: any change in parameter or setting will instantly update the simulated spectrum and give visual feedback to decide if the current parameters are good starting values for a fit. (Links to all programs are listed in SI).

Fitting EPR spectra is a difficult problem. The investigator needs to decide on a model that is reasonable and sufficient, then interpret the result in terms of

that model. Often several models can result in a reasonable approximation of the measured lineshape. The fitting of an experimental spectrum can be described as an algorithm guided sequence of lineshape simulations, starting with reasonable guesses of the fitting parameters. Once fitting starts, the fitting algorithm will systematically vary the parameters to find new values that make the agreement between data and simulation better until no more improvements are possible.

The development of the present lineshape fitting programs has passed through several stages that have been shaped by the specific application at the time. The programs initially developed by the Freed group were for application to well-characterized systems: for example, simple liquids or solutions that could be studied as a function of temperature [67] or pressure [68]. Later modifications were made to enable characterization of spin probes on surfaces [69] or in liquid crystals [70, 71] and liquid crystalline phases of lipid membranes [72]. Consequently, many of the features of the programs such as non-Brownian diffusion, discrete jump, and anisotropic viscosity models do not apply to spin-labeled biomolecules such as proteins and nucleic acids, where the dynamics are well-represented as Brownian motion. Here we will focus on the features most useful for application to biomolecules.

The program MultiComponent is a standalone program to simulate and fit EPR spectra. The core computations are based directly on the Fortran code described by Schneider and Freed [27] and implemented for fitting by Budil et al. [28] while the UI and fitting algorithms are written in LabVIEW. Details can be found in the SI. While it has been used for decades by many researchers, there was never a publication or good guidelines. This article tries to rectify that but will focus on features that apply to nitroxide spin labels. Details, pitfalls, limitations and outlook will be discussed.

Given an EPR spectrum of a nitroxide attached to a protein, typically a lot of metadata is known to aid in selecting an appropriate model. This includes the spin label chemistry, the type of protein (size, water soluble, membrane, etc.), its environment (buffer, detergent, lipids, etc.), and the experimental conditions (temperature, pressure, presence of ligands, etc.). Validation should also be made to ensure the raw data is reasonable, for example the number of spins should match the protein concentration. If the spectrum is much weaker, maybe all we see are artifacts from spin labeled impurities. Sometimes there is a small fraction of unreacted spin label or misfolded or aggregated protein. The result of a fit is highly multidimensional and should always be interpreted in simpler terms that are sufficient to answer the relevant questions. Other EPR techniques such as accessibility studies and pulse methods can sometimes be helpful to round out the picture. It should always be possible to show the results in a simple graph with few dimensions.

The investigator might be confronted by two experimental spectra as shown in Fig. 2, where the same spin labeled protein has been recorded under two different conditions. Each spectrum contains two interesting components and two irrelevant components, and we are interested in how the ratio of the two interesting

components depends on condition while the exact magnetic parameters are not of primary interest.

5 Using the Multicomponent Program

After installation, the program MultiComponent is ready to run. Details of the program algorithms and implementation are available in the supporting document (SI). Briefly, the single-spectrum computation is based directly on the original Fortran code, retaining all parameters as defined in reference [28], while the UI and fitting algorithms are written in LabVIEW (National Instruments). Highly efficient code and extensive parallelization makes simulation and fitting very fast. This section will first introduce the user interface and data structures to aid in navigation and understanding of the program. Online help is accessible from within the program, and the user is encouraged to refer to it. Minor details can change as the program is updated and features added (see SI for some possibilities).

5.1 The User Interface

While the user interface is very rich, care has been taken to group parts into logical sections consisting of several nested tab structures. Even without available experimental data, simulation can be made immediately, or the fitting procedures tested using the built-in default data or any simulated data.

To simulate a spectrum, we first need to get familiar with the data structures and parameters. While there are very detailed options to fine-tune the fitting algorithms, the defaults are usually fine to start, focusing on the spectrum instead. Note that any change in parameter or settings will recalculate the spectrum based on the new values for instant user feedback.

5.2 The Parameters

Each spectrum component depends on several classes of parameters: (1) magnetic parameters, including the electronic g -factor, the hyperfine interaction between the electron and a single major nucleus, and inhomogeneous linewidth parameters; (2) dynamic parameters, including rotational diffusion rates, Heisenberg exchange, and orienting potential coefficients, (3) fixed parameters that specify the diffusional model and may not be varied in a fitting procedure, and (4) basis set parameters that govern the accuracy and speed of the calculation.

Most of the parameters in the MultiComponent user interface retain the naming convention from reference [28] verbatim. This article will focus primarily on a subset of parameters most relevant for fitting nitroxide spin labels on biomolecules. These are described in greater detail below. For an explanation of other parameters, the reader is referred to references [27, 28]. A detailed and annotated table is also available in SI.

5.3 Tensors and Tensor Representations

Although most parameters in MultiComponent are scalar, there are four sets of parameters that represent anisotropic properties related to the structure of the spin probe and require special mention. Three of these are magnetic tensors (\mathbf{g} for the electronic g -factor, \mathbf{A} for the nuclear hyperfine interaction, and \mathbf{W} for linewidth broadening) that are determined by the electronic distribution on the label, and one is the rotational diffusion tensor \mathbf{R} that is determined by the hydrodynamic shape and local geometry of the label. Each tensor has three principal values associated with each of three Cartesian directions in an axis system that is fixed relative to the molecular structure of the label. In principle, none of these axis systems need coincide, so the program use the \mathbf{g} axes as a reference system and specifies the others relative to that. For nitroxides, the g_x -axis is taken to lie along the N–O bond and g_z along the axis of the nitrogen p -orbital. The \mathbf{W} axes are assumed to coincide with the \mathbf{g} axes. The relative orientations of the \mathbf{A} and \mathbf{R} tensors are given by the so-called magnetic and diffusion “tilt angles” which are simply the standard Euler angles (α, β, γ) that specify the rotation of a body in 3-dimensional space. [28]

The principal components of any of these tensors are generally expressed relative to a set of Cartesian axes, so that tensor \mathbf{T} has principal values T_x, T_y , and T_z . However, it often occurs that a tensor is not fully asymmetric ($T_x \neq T_y \neq T_z$), the asymmetry cannot be experimentally resolved, or one or two components of the tensor are known and may be fixed during a fitting procedure. For such cases, MultiComponent offers two alternative conventions for specifying tensor principal values.

The first alternative is the so-called “modified spherical tensor” form, which consists of an isotropic component (average of T_x, T_y , and T_z), an axial component (difference between T_z and the average of T_x and T_y) and a rhombic component (difference between T_x and T_y), respectively denoted as T_1, T_2 , and T_3 . Thus, for example, an axial hyperfine tensor would be represented with $A_2 \neq 0$ and $A_3 = 0$. This form has special implications for the rotational diffusion tensor, whose elements are base 10 logarithms of the rotational rate constants in seconds. Thus the average component R_1 represents the *geometric mean* of the rotational rates around the three Cartesian axes, $R_1 = \log_{10} (R_x R_y R_z)^{1/3}$; the axial component is the *ratio* of the mean rate around x and y to the rate around z : $R_2 = \log_{10} (\sqrt{R_x R_y} / R_z)$; and the rhombic component is the ratio of the rates around x and y : $R_3 = \log_{10} (R_x / R_y)$.

The second alternative tensor representation is a mixed form unique to MultiComponent, consisting of the components T_1, T_z , and T_3 as already defined above. This feature accommodates the common situation that the isotropic values of the \mathbf{A} and \mathbf{g} tensor (A_1 and g_1) are known from a liquid solution spectrum of the spin label, and A_z is known from a frozen solution spectrum. In this case, A_1 and A_z may be fixed during the fitting of a slow-motion spectrum and only A_3 varied, effectively varying A_x and A_y in a correlated way to keep A_1 and A_z constant. This can reduce the number of parameters needed for fitting, especially important at X-band. The transformation matrices to convert between these different representations are listed in the SI. The flexible user interface for tensors is shown in Fig. 5.

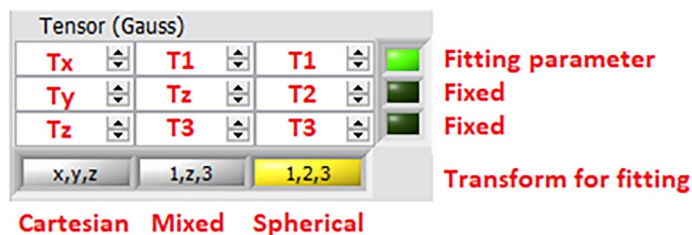


Fig. 5 The tensor user interface as implemented. The columns represent the three available transforms. Any element can be changed, and the other columns will instantly be recalculated. For example, if T_x is changed, T_1 , T_2 and T_3 are adjusted accordingly. It is important to note that changing T_1 or T_3 has a different effect when done in the second or third column because the invariant elements are different in the two cases. The choice of transform and selected fitting parameter(s) is only relevant for fitting. In the shown case, fitting is done in the spherical coordinate system and only T_1 is a fitting parameter while T_2 and T_3 are held constant. This also means that during fitting, T_x , T_y , and T_z are simultaneously varied to agree with the spherical values at any time

5.4 The Data Structures

All parameters that define the spectrum can be found on the “EPR parameters” tab and its sub-tabs where they can be changed and optionally selected for fitting. MultiComponent greatly facilitates the fitting of multiple spectral components (Fig. 2), which is common in investigations of spin-labeled biomolecules. The program allows up to four spectral components designated by letters (A, B, C, D). There are also four parameter sets designated by numbers (1, 2, 3, 4). Individual tensors and groups of parameters in each set may be freely assigned to any component so that selected parameters may be shared by different components. This feature makes it possible to analyze multiple species in situations that often occur in biochemical systems, for example two components with the same magnetic parameters but different mobilities, such as a single type of probe in two different environments, or two species with different magnetic properties, with the same dynamic parameters, such as an ^{14}N and an ^{15}N nitroxide in the same phase.

The “EPR Parameters” tab is organized into four sub-tabs arranged according to typical work flow: (1) the “Global Settings” sub-tab, which contains the global parameters described above and an assignment table that allows selection of active spectral components and assignment of specific parameters and parameter groups to each component; (2) the “Tensors” sub-tab, which allows selection of \mathbf{g} , \mathbf{A} , \mathbf{R} , and \mathbf{W} tensor components and forms for each of the four parameter sets; (3) the “Parameters and Settings” sub-tab, which contains a number of additional parameters for each of the four parameter sets that are discussed further below, and (4) the “Tweaks” sub-tab, which contains parameters for small hyperfine interactions on the nitroxide and field modulation.

As mentioned above, most parameters in the “Global Settings” sub-tab apply equally to all components of the composite spectrum. While parameters describing the spectrometer microwave frequency and field settings are fixed, the microwave phase and field shift may be varied in the fitting procedure.

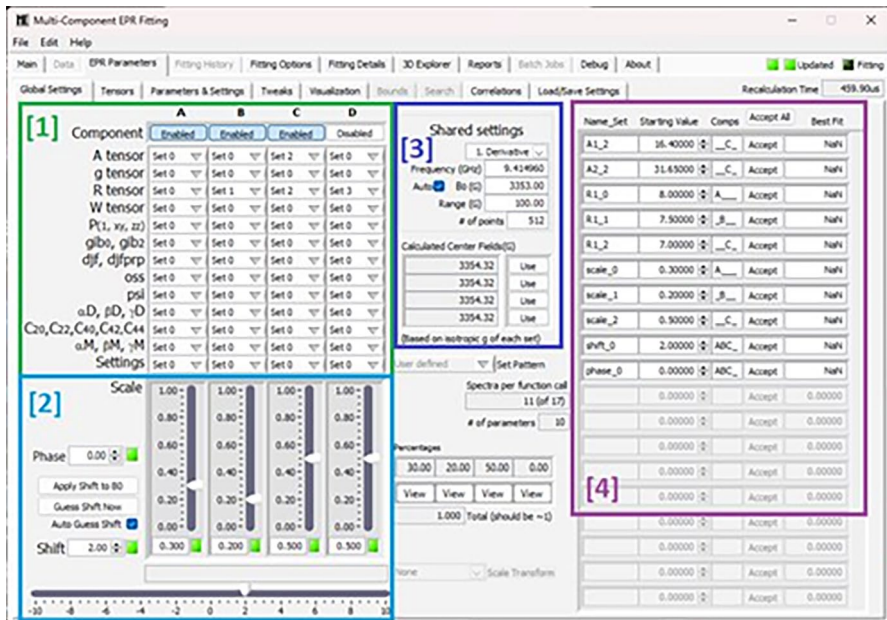


Fig. 6 The main parameter selection interface. (1) Set assignment table: In this case, three spectral components are active. A–C Each component uses a different set for the rate tensor (Set 0, Set 1, or Set 2). Components A and B share all other parameters and settings while component C has its own A tensor from set 2. (2) Amplitudes, shift, and phase: all components have their own scale factor. Shift and Phase are applied globally and are always shared by all active components. (3) Shared settings: here are global settings, such as the microwave frequency, center field and field range and derivative. By default, the center field is adjusted automatically when the frequency is changed, based on g_1 of the first set. (4) Fitting parameter summary: this table shows all parameters and their starting values that are currently selected for fitting. The parameter name is followed by a number, indicating the set. The Comps column shows which components use each parameter. In this case, there are ten fitting parameters, A1(set3) and A2(set3) are exclusively used by component C. R1 (set 0) is used by component A and R1(set1) is used by component B and R1(set3) is used by component C. Each component has its own scale parameter, while shift and phase are always shared by all three components. Scaling is never shared. Once fitting is complete, the best fit parameters will populate the last column. Pressing [Accept] at this point will copy the best fit as new starting parameters and update all relevant controls on the tensor and parameter tabs

The “Global Settings” sub-tab also displays a table that shows each parameter selected for fitting by its name and set number, its starting values, and the components (ABCD) that use it. Parameters can be changed directly in the table and the simulated spectrum is immediately updated to reflect that change. See Fig. 6 for a detailed description.

In the “Tweaks” sub-tab, additional small hyperfine interactions may be included in the simulated spectrum, but these are not variable parameters. Up to three groups of equivalent protons may be included as well as an additional ^{13}C or ^{14}N nucleus to account for the ^{13}C wings that are visible in very fast motion

spectra or for nitroxides that have a second distant nitrogen in the ring, respectively. Broadening due to field overmodulation can also be applied in this sub-tab. MultiComponent creates a single kernel convoluting all tweaks, which is then convoluted with the simulated spectrum. Consequently, these parameters apply to all active components equally.

6 Simulations

The shape of a single EPR spectrum depends on a huge amount of magnetic and motional parameters. MultiComponent is facile enough to let new users get a feeling for how the spectrum changes as a function of each parameter of interest. A seasoned EPR spectroscopist can look at a spectrum and leverage years of experience to immediately do a quick analysis summarized in a few words (e.g., “looks isotropic with a certain correlation time”, “looks like R1 located on an alpha helix surface site”, “must be an internal site with little motion”, “has two states in equilibrium”, etc.). In the future, maybe a trained AI system will be able to do the same, but at this time everybody is encouraged to just play with the program. Even without experimental data, the student can test and see from first experience how each parameter is reflected in the spectrum. MultiComponent allows any given simulation to be loaded back as data, optionally with simulated noise, so that one of the parameters may be changed to observe its effect or to see if fitting can successfully recover the known parameters from intentionally incorrect starting values. There is even a 3D visualization to show how the spectrum changes as a function of one selected parameter. Most default values are reasonable, but there is no input validation and unreasonable choices can be entered. If things get out of hand, the defaults can be reloaded.

To explore the lineshape as a function of interesting parameters, some simple cases could be investigated as an exercise as follows:

6.1 Isotropic Motion as a Function of Rotational Rate R1

Here R2 and R3 must be zero, i.e., $R_x=R_y=R_z$. Using all defaults, select just one component (e.g., Component A) on the parameter summary page, then go to the tensor page and change R1 in the last column of the R tensor panel to keep the rate isotropic (i.e., $R_2=R_3=0$). Changing R1 in the second column would introduce anisotropy because R_z is held constant in that case. (Refer to Fig. 5).

The spectrum as a function of any single fitting parameter can be visualized in 3D over a selected range to aid in exploring its effect on the lineshape. Figure 7 shows how an isotropic X-band spectrum varies as a function of isotropic rate.

6.2 Simple Anisotropic Motion

A simple deviation from isotropic motion is the introduction of axial anisotropy where rotation about one of the molecular axes is faster. In the limiting case of

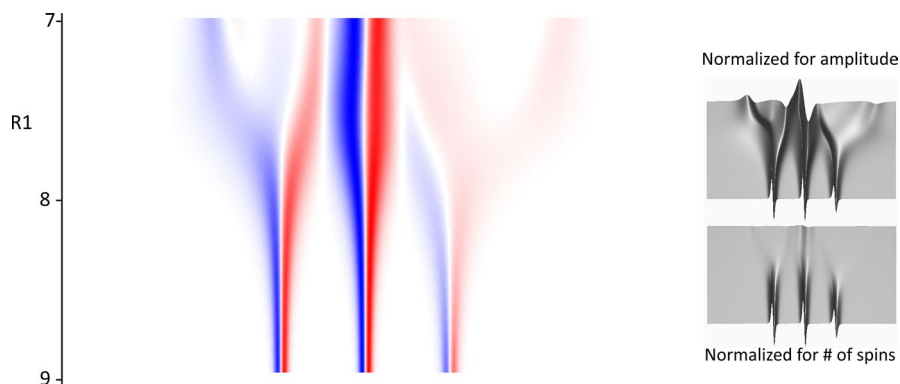


Fig. 7 A 3D illustration shows how the first derivative X band EPR spectrum changes as a function of isotropic rate. Field range is 10 mT. Left: A shaded top view where red is negative, and blue is positive. Right: A 3D surface of the same data viewed at an angle. If the spectra are normalized to the number of spins (bottom right) the more immobile spectra have significantly lower amplitude. (The 3D Explorer in MultiComponent can be used to visualize the spectrum dependence on any single fitting parameter. The view and shading can be changed to produce the above images.)

infinitely fast motion around one arbitrary axis and no rotation around the others, the spectrum can be simulated as a rigid limit spectrum with effective tensors for \mathbf{A} and \mathbf{g} that can be calculated [73] using the Euler angles defining the axis of rotation. This is implemented in the companion program RigidLimit where the angles and order parameters can be entered (see SI for link).

MultiComponent can be used to simulate the more general case where the rates are intermediate. Here \mathbf{R} is anisotropic, i.e., R_2 is nonzero. A positive R_2 means that

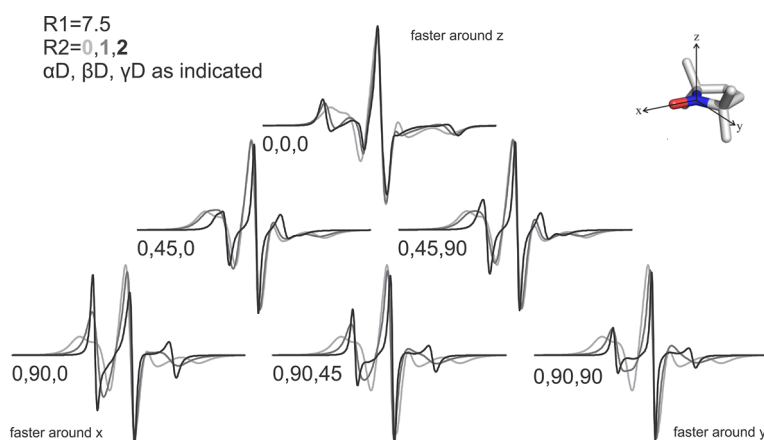


Fig. 8 Axial anisotropy: A representative collection of spectra that all have the same geometric average of the rate tensor. Assuming axial symmetry and anisotropic motion, the axis of the faster rotation is defined by the diffusion tilt angles as shown. The rotation around the fast axis is $10\times$ (gray) or $100\times$ (black) faster than the rotation around the two other axes. For comparison, the isotropic case is also shown (light gray)

rotation around the diffusion z axis is faster than around x and y . If $R_3 = 0$, then rotational rates around x and y are equal and we have axial symmetry. It is quite rare that rotation around the unique axis is slowest, so R_2 should be kept positive.

In the case of significant rotational anisotropy, the EPR lineshape is also dramatically affected by the orientation of the fast rotation axis relative to the molecular frame of the nitroxide. This is illustrated in Fig. 8, which compares spectra with the same average rotational rate but axial anisotropy where rotation around the fast axis is 10 or 100 times faster than rotation around the two other axes. The z diffusion axis is oriented along the magnetic x , y , and z axes and halfway between each pair of axes, indicated by the diffusion tilt angles (α_D , β_D , γ_D). The substantial changes in line shape with diffusion tensor orientation underscore the strong dependence of the EPR lineshape on these parameters. Consequently, the geometry of the label tether and other hydrodynamic properties of the label should be carefully considered in setting the initial orientation of the diffusion axes.

6.3 The MOMD Model

Spin labels attached to a biomolecule are inherently constrained in their motion by the covalent bonds linking them to the macromolecule as well as by interaction with nearby side chains of that macromolecule. A model that has been adapted from the early applications of the EPR line shape fitting programs for application to spin-labeled biomolecules is that of microscopic order, macroscopic disorder (MOMD) [25, 74, 75]. This model was originally applied to nematic phases such as membranes, in which the spin label or probe is ordered with respect to a unique axis called the “director” of the nematic phase, but individual membrane domains with local nematic order are randomly oriented throughout the sample. This is analogous to a protein that is randomly oriented in the laboratory frame while imposing local ordering on the attached label.

The local ordering of the spin label is imposed by a potential energy function that is expressed as a weighted sum of spherical harmonic functions that are defined in the principal axis system of the rotational diffusion tensor \mathbf{R} . This potential energy function thus determines the distribution of the director orientation in the rotational diffusion frame. The potential weighting coefficients c_{LK} in MultiComponent scale spherical harmonic functions of degree L and order K , and are limited to the set (c_{20} , c_{22} , c_{40} , c_{42} , c_{44}). A detailed description and graphical depictions of the influence of these coefficients on the director distribution may be found in reference [75]. MultiComponent provides a similar real-time visualization of these effects on the “Visualization” sub-tab of the “EPR Parameters” tab, but the distribution is shown relative to the molecular (\mathbf{g} tensor) axes and shows the combined effect of the potential coefficients and diffusion tilt angles. New users are encouraged to play with this visualization to get a feeling for the effects of an orienting potential.

To account for macroscopic disorder, the MOMD spectrum must be integrated over all orientations of the local director axis in the laboratory frame. Since the potential function is uniaxial, the integration only needs to be taken over the so-called “director tilt” angle, ψ .

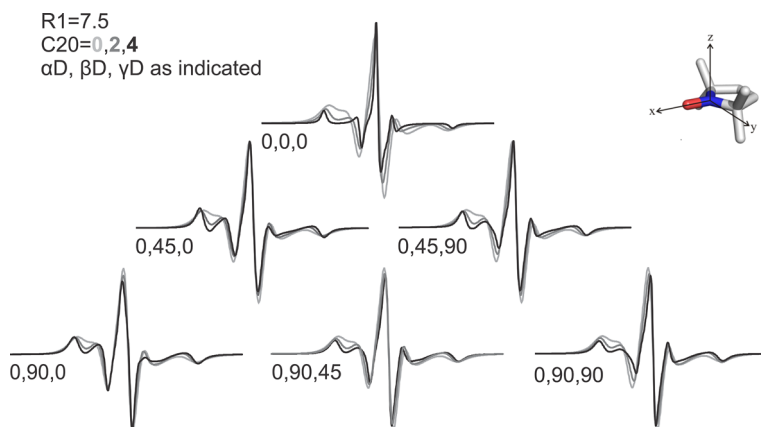


Fig. 9 MOMD ordering: A representative collection of spectra that all have the same isotropic rate but differ in the degree, direction, and magnitude of ordering. Assuming isotropic motion, the direction of ordering is defined by the diffusion angles as shown. The magnitude of the C20 potential is 2 (gray) or 4 (black) compared to the absence of ordering (light gray)

The effect of local ordering on the EPR spectrum can qualitatively resemble that of rotational anisotropy even when the rotational diffusion tensor is isotropic, as shown in Fig. 9. In this figure, the ordering z axis is oriented along each of the magnetic axes and halfway in between each pair. In each case, a potential with $c_{20}=2kT$ or $4kT$ is present, resulting in a distribution of directors that is centered on the diffusion z axis, but different magnetic axes are aligned with the diffusion tensor depending on the orientation of the diffusion axes in the magnetic frame.

Historically, $\beta_D=36^\circ$ has been used when modeling the R1 label on a protein [38] and it is still considered a good starting point for R1 and similar labels. Figure 10 shows the effect of ordering for this orientation as a function of isotropic rate and c_{20} potential.

Remarkably, in the MOMD model, the spectrum is often only weakly dependent on the orientation of the ordering axis (i.e., the diffusion z axis). An illustrative example is given in Fig. 11 where the diffusion z axis is aligned with magnetic x or

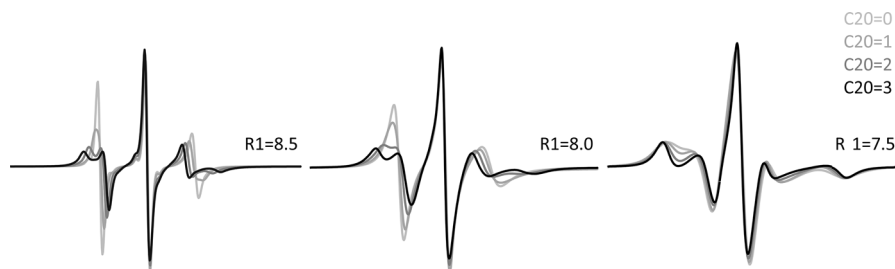


Fig. 10 An example showing how the MOMD spectrum changes as a function of rate and order for a commonly used orientation ($\alpha_D=0$ degrees, $\beta_D=36$ degrees, $\gamma_D=0$ degrees)

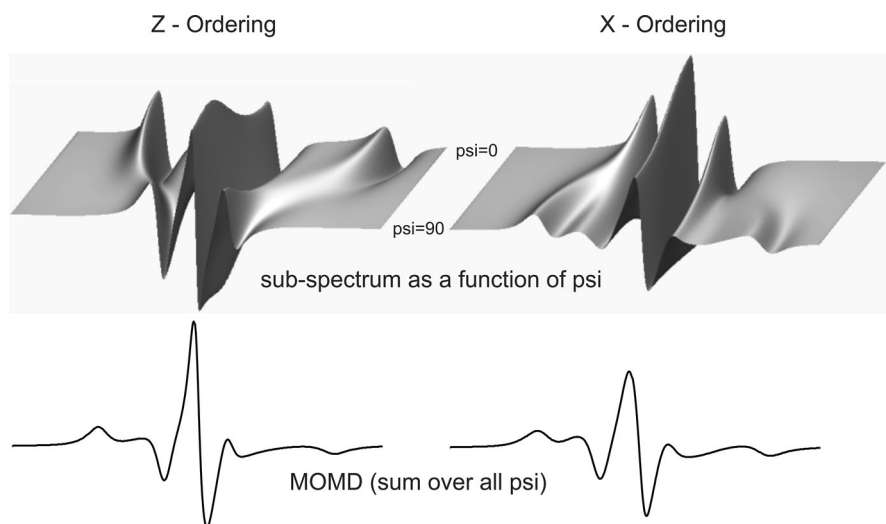


Fig. 11 The origin of the MOMD lineshape as a function of psi dependent sub-spectra for two ordering orientations

z , respectively. While the sub-spectra along the director are quite different, they sum to a relatively similar MOMD spectrum.

In the most general case, rate and order can be combined in near infinite possibilities using anisotropic motion, orientations, and several potential terms but it is recommended to keep it simple. Each ordering potential can be positive or negative. Any given set of potentials and tilts can be inspected on the visualization tab. Terms for the potentials can in principle be obtained from molecular dynamics simulations [76, 77] and used to validate the model.

7 Fitting

Once an experimental spectrum is loaded into the program, the simulation with the current parameters is overlaid and the difference is also displayed. At this point it is useful to identify the major points of disagreement and manually adjust suitable parameters to get reasonable starting values. For example, R_1 could be changed, or a second component added to see if the simulation better resembles the experimental spectrum. Pressing the [Fit] button (or just pressing the [home] button on the keyboard) will have the fitting algorithms trying to find better values for the selected fitting parameters.

While currently 134 parameters can be simultaneously enabled for fitting, it is crucially important to select only a very small subset, keeping most parameters at reasonable fixed values. Even if there are multiple components, parameters can be

shared to keep the problem reasonable. An important tool is the correlation matrix which will identify the presence of parameter correlations. If parameters are strongly correlated, the fit is unlikely to converge to anything that makes sense. Refer to the SI for a table to see which parameters are relevant for nitroxides.

8 Fitting Walkthrough

Given an experimental spectrum, the question arises how to approach fitting. It is best to start with the simplest model and fewest number of variable parameters, then adjust to improve the fit. These adjustments included adding more fitting parameters, more spectral components, and/or using a more complicated model for any component that needs it. Don't be fooled by the lineshape, sometimes a single MOMD component might look to the untrained eye like a spectrum with two or more non-MOMD components.

While it is true that throwing more and more parameters at a problem will improve the fitting result, it makes little sense if the parameters are highly correlated or do not mean anything. Often, an approximate result with useful parameters is better than a near perfect fit with a vast collection of nonsensical parameters.

1. Start with one isotropic component.
2. Is there a very mobile component (free label in solution)? Maybe it can be added as a new component, edited out or masked.
3. Add a second isotropic component differing only in rate. Better?
4. Where are the problem areas? (Maybe $[A]$ or $[g]$ is slightly off. Does fitting for $A1$ improve things? How about $g2$?)
5. Can the spectrum fit be improved by including anisotropy ($R2$ and e.g., βaD)
6. If one component is very immobilized, do we see oscillations? Do they go away if we increase the truncation parameters?
7. How about going back to a faster isotropic rate but adding an orienting potential (MOMD)?
8. If MOMD causes oscillations (noticeable when potential coefficients are large), the number of orientations (NORT) needs to be increased.
9. A thoughtful balance of "rate" versus "order" can only be achieved with a detailed analysis comparing several approaches.

9 Fitting Guidelines

Fitting an EPR spectrum and selecting reasonable starting parameters and models is not simple and choices might be guided by bias and incorrect assumptions. It is important to try several models and look at the results critically. The inherent speed of the fitting allows quick testing and comparison of many models.

This section discusses some important points to keep in mind. Highly correlated parameters can give unreasonable results where one parameter can drift outside any reasonable range while a second, highly correlated parameter can correct for that by going into an equally unreasonable value while not really making the fit worse. Additional line broadening can be caused by many experimental artifacts and deserves detailed discussion.

9.1 Parameter Correlations

It is always important to keep an eye on parameter correlations and there is a special tool to inspect them for any parameter selection. The correlation tab will calculate the correlation matrix for the currently selected fitting parameters at their current value. This allows us to estimate if any parameters are strongly correlated. After a fit has completed, the final correlation matrix will be determined for the best fit values automatically and displayed on the "Fitting Details" tab. The "EPR Parameters... Correlations" tab allows us to estimate correlations from the starting values before fitting.

The correlations are displayed as a matrix containing all possible pairwise parameter combinations. The values are in the range from -1 to 1 , where 0 means no correlation, -1 means 100% negatively correlated, and 1 means 100% positively correlated. The background color has a red tint proportional to the absolute correlation value. Troublesome correlations show in dark red! A correlation shows how well the change in one parameter can be compensated by a change in another parameter for a nearly equally good fit.

All parameters are correlated to some degree. For example, an increase in rate increases the amplitude of the central line that can be somewhat (but not perfectly!) compensated for by a decrease in scale. Rate and scale are thus correlated with a negative value. Even a relatively strong correlation might be acceptable, but if two parameters are highly correlated (e.g., $|r| > 0.95$), one of them needs to be fixed at a reasonable value to successfully fit for the other.

In EPR, a very strong correlation exists between the isotropic g value (g_1) and the shift parameter, because they both move the spectrum left or right without changing the lineshape much. The correlation between " g_1 " and "shift" will be close to 1.0 . (Note, however, that if there are multiple components and only one of them fits for g_1 , the strong correlation can obviously disappear). Also note that the DLL code has no input for the microwave frequency and the original shift parameter just designates an offset from the isotropic g value. In MultiComponent, the MW frequency is explicit and a change in g_1 will shift the spectrum by internally calculating a virtual shift that is not exposed to the user. By default, a change in frequency will correctly shift the field axis to keep the spectrum in view.

Correlations might depend on the values of other parameters. For example, A_x , A_y , and A_z will be highly correlated to each other for fast motion, but uncorrelated for slow motion. For fast motion, only fit for A_1 , the isotropic average because A_x , A_y , and A_z could differ significantly but produce the same spectrum as long as their

average is A_1 . The g anisotropy nearly collapses for experiments at low microwave frequencies while becoming dominant at very high frequencies.

Use the correlation tool to potentially identify correlations between the parameter estimates but note that the correlations could be different at the best fit values.

The diagonal elements of the covariance matrix together with the estimated noise in the data are used to estimate parameter errors, assuming that the model is appropriate, and the residual (data-fit) is pure gaussian noise. If the fit is poor, the error estimates are meaningless. Note that correlations and parameter error estimates are also calculated when using fitting algorithms that do not internally use partial derivatives, such as Nelder-Mead and Monte Carlo.

9.2 Line Broadening

There are many factors that affect line broadening in the most generic sense. They all “broaden” the spectrum one way or another, so they are all somewhat correlated. Some are rigorous, but some are due to artifacts, and it is important to understand the difference. Two are implemented in the core DLL code as the **W** tensor (Lorentzian) and the **gib0** parameter (Gaussian).

An external addition is modulation broadening, allowing one to get better parameter estimates in the presence of overmodulation. The need for this originated from lab members that, for very noisy samples, struck a balance between modulation distortion and noise, preferring less noise. For modern Bruker spectrometers the modulation amplitude is exactly known because the modulation coils of cavities and resonators are factory matched and calibrated. This is not always true for the ancient Varian spectrometers where factory and home-built modulation coils had to be matched and calibrated manually. Often, the setting on the modulation dial did not exactly reflect the actual modulation amplitude and needed to be guessed or measured explicitly. If modulation artifacts are suspected, testing is recommended to see if setting a reasonable modulation amplitude improves the fit. Because all types of line broadening are somewhat correlated, the decision was made for the modulation amplitude to be a fixed setting.

Gib0 is a Gaussian approximation to the inhomogeneous broadening due to the nearby protons. Alternatively, this can be modeled by explicit proton splitting based on the number of neighboring protons. For a sufficient number of equivalent protons, a Gaussian envelope is a good approximation, but if some protons are not equivalent this approximation is no longer valid. For example, the nitroxide group of R1 has 12 equivalent methyl protons, but also one ring proton away by the same number of bonds, which is not equivalent. The proton splitting on the tweaks page cannot be an adjustable parameter, but when enabled, we can still fit for **Gib0** as additional broadening, taking note that we only fit for the residual balance. The defaults are reasonable, but not rigorous.

Many experimental artifacts can contribute to line broadening, and some will manifest in artificial increases of **gib0** or **W**, so can still be fit with reasonable agreement.

- *Modulation broadening*: slight overmodulation can be partially compensated by the highly correlated parameter g_{ib0} . If the modulation amplitude is known or can be guessed, it is better to set the modulation amplitude under tweaks.
- *Saturation broadening*: too much microwave power, especially noticeable if care is not taken when recording samples with very long spin lattice relaxation time (T_1), will cause saturation broadening reflected in \mathbf{W} . It is recommended to obtain a saturation curve to ensure that the microwave power is low enough. Note that in solution, the presence of dissolved oxygen is beneficial and relieves saturation broadening by reducing T_1 and the power can be increased for better signal/noise. Since $T_2 \ll T_1$ for nitroxides on proteins, we have the somewhat anti-intuitive case where the presence of a “broadening agent” relieves this type of broadening and sharpens the line if the same microwave power would be slightly too high in the absence of oxygen.
- *Collision broadening*: collisions with fast relaxing paramagnetic agents in solution shorten T_2 and cause broadening if the collision frequency gets into the T_2 range. In most experiments, dissolved oxygen is present, especially noticeable in a hydrophobic environment such as in lipid membranes or organic solvents where oxygen solubility is high. Collision broadening is reflected in an artificial isotropic increase in \mathbf{W} . This is Heisenberg exchange with fast relaxing species and distinct from the Heisenberg exchange modeled by the “oss” parameter.
- *Dipolar broadening*: if the nitroxide spins are not sufficiently dilute, neighboring spins can cause dipolar interactions. This can be due to aggregation, dimer formation, or other scenarios where nitroxides are close. In the absence of orientation selection, the broadening function for each exact distance is a Pake function <https://sites.google.com/site/altenbach/labview-programs/epr-programs/short-distances?authuser=0>, but in the case of weak interactions and a wide distance distribution it cannot easily be distinguished from other types of broadening. Often there is also orientation selection, making exact solutions very complex [78]. A control experiment would be to label the protein with a mix of nitroxide label and diamagnetic analog to dilute the spins [32].

9.3 Baseline Artifacts

Due to the use of field modulation, the spectrum is recorded as the first derivative and even small baseline artifacts or over- or under-correction of the baseline during post processing can be problematic. Double integration is very sensitive to these errors. More severe artifacts originate from impurities in the sample and even the sample cell or resonator components. For example, quartz capillaries that were X-rayed during shipping can develop lattice defects containing unpaired electrons, contributing to the background. When ordering capillaries, it is important to avoid shipping by air. Some sealants also have background signals, this includes some batches of Critoseal[®] (McCormick Scientific) or the red wax used in early studies. Even flame sealing can potentially introduce signals. It is important to keep the sealant portion outside the active resonator volume. Some high-pressure studies require

the use of pressure-tolerant ceramic cells [79]. These often have paramagnetic impurities that contribute to dramatic background distortions.

9.4 Other Artifacts

Some loop gap resonators have a slight phase problem and contain a few degrees of dispersion. It is important to fit for the phase.

Within limits, a faster motion can be simulated by lowering the effective A and g tensor to more averaged values. To get good estimates of the rates, the tensors should be kept at values reasonable for the environment. Similarly, if a spectrum is very immobilized small changes in rate can be masked by slightly different environment polarity.

10 Summary

EPR spectra of nitroxides attached to a protein have very rich information but are also often ambiguous. The researcher needs to decide what information is relevant to answer the questions about the system under study. Most of the time, close, but not perfect, fits are sufficient. MultiComponent can be used to quickly get a good approximation of the lineshape, and thus the relevant parameters needed to include or exclude certain prior assumptions about the protein model. Most important is the study of lineshape changes as a function of conditions, giving the type, direction, and possibly magnitude of the concomitant structural changes. To get thermodynamic parameters as a function of state, only relative amounts of each component are required, and a good fit of component fractions is then more important than the parameter details.

Because the first derivative display tends to amplify small differences, equilibrium studies that require the determination of relative component amounts, the results tend to be quite accurate even if the fit is only approximate.

If suitable instruments are available, experiments could be repeated at different microwave frequencies. For example, the g anisotropy is much better defined when going way above X-band.

The program MultiComponent is still in active development and new features are regularly added. The user should refer to the website for details. A list of possible feature additions is listed in the SI.

Supplementary Information The online version contains supplementary material available at <https://doi.org/10.1007/s00723-023-01610-2>.

Author Contributions CA wrote outline, some sections and made figures, DB wrote some sections. Both discussed and reviewed all sections.

Funding Funding for CA was from the Jules Stein Endowed chair to Wayne L. Hubbell and the SEI software core program. DB declares no funding.

Availability of Data and Materials The installer for the program MultiComponent can be freely downloaded from the Hubbell Lab Software Page (<https://www.biochemistry.ucla.edu/Faculty/Hubbell/software.html>). The MultiComponent product page and online help can be accessed from within the software and is located here (<https://sites.google.com/site/altenbach/labview-programs/epr-programs/multicomponent?authuser=0>).

Declarations

Conflict of interest The authors declare that they have no conflict of interest.

Ethical Approval N/A (there are no human or animal studies involved).

Open Access This article is licensed under a Creative Commons Attribution 4.0 International License, which permits use, sharing, adaptation, distribution and reproduction in any medium or format, as long as you give appropriate credit to the original author(s) and the source, provide a link to the Creative Commons licence, and indicate if changes were made. The images or other third party material in this article are included in the article's Creative Commons licence, unless indicated otherwise in a credit line to the material. If material is not included in the article's Creative Commons licence and your intended use is not permitted by statutory regulation or exceeds the permitted use, you will need to obtain permission directly from the copyright holder. To view a copy of this licence, visit <http://creativecommons.org/licenses/by/4.0/>.

References

1. A.P. Todd, J. Cong, F. Levinthal, C. Levinthal, W.L. Hubbell, Site-directed mutagenesis of colicin E1 provides specific attachment sites for spin labels whose spectra are sensitive to local conformation. *Proteins Struct. Funct. Genet.* **6**(3), 294–305 (1989). <https://doi.org/10.1002/prot.340060312>
2. W.L. Hubbell, W. Froncisz, J.S. Hyde, Continuous and stopped flow EPR spectrometer based on a loop gap resonator. *Rev. Sci. Instrum.* **58**(10), 1879–1886 (1987). <https://doi.org/10.1063/1.1139536>
3. C. Altenbach, S.L. Flitsch, H.G. Khorana, W.L. Hubbell, Structural studies on transmembrane proteins. 2. Spin labeling of bacteriorhodopsin mutants at unique cysteines. *Biochemistry* **28**(19), 7806 (1989). <https://doi.org/10.1021/bi00445a042>
4. C. Altenbach, T. Marti, H.G. Khorana, W.L. Hubbell, Transmembrane protein structure: spin labeling of bacteriorhodopsin mutants. *Science* (Washington, DC, 1883–) **248**(4959), 1088 (1990). <https://doi.org/10.1126/science.2160734>
5. D.A. Greenhalgh, C. Altenbach, W.L. Hubbell, H.G. Khorana, Locations of Arg-82, Asp-85, and Asp-96 in helix C of bacteriorhodopsin relative to the aqueous boundaries. *Proc. Natl. Acad. Sci. USA* **88**(19), 8626 (1991). <https://doi.org/10.1073/pnas.88.19.8626>
6. C. Altenbach, K. Yang, D.L. Farrrens, H.G. Khorana, W.L. Hubbell, Structural features and light-dependent changes in the cytoplasmic interhelical E–F loop region of rhodopsin: a site-directed spin-labeling study. *Biochemistry* **35**(38), 12470–12478 (1996). <https://doi.org/10.1021/bi960849i>
7. W.L. Hubbell, C. Altenbach, C.M. Hubbell, H.G. Khorana, Rhodopsin structure, dynamics, and activation: a perspective from crystallography, site-directed spin labeling, sulfhydryl reactivity, and disulfide cross-linking. *Adv. Protein Chem.* **63**, 243–290 (2003). [https://doi.org/10.1016/s0065-3233\(03\)63010-x](https://doi.org/10.1016/s0065-3233(03)63010-x)
8. C. Altenbach, A.K. Kusnetzow, O.P. Ernst, K.P. Hofmann, W.L. Hubbell, High-resolution distance mapping in rhodopsin reveals the pattern of helix movement due to activation. *Proc. Natl. Acad. Sci. USA* **105**(21), 7439–7444 (2008). <https://doi.org/10.1073/pnas.0802515105>
9. K. Palczewski, T. Kumasaka, T. Hori, C.A. Behnke, H. Motoshima, B.A. Fox et al., Crystal structure of rhodopsin: a G protein-coupled receptor. *Science* **289**(5480), 739–745 (2000). <https://doi.org/10.1126/science.289.5480.739>

10. G.F.X. Schertler, Structure of rhodopsin and the metarhodopsin I photointermediate. *Curr. Opin. Struct. Biol.* **15**(4), 408–415 (2005). <https://doi.org/10.1016/j.sbi.2005.07.010>
11. J. Standfuss, P.C. Edwards, A. D'Antona, M. Fransén, G. Xie, D.D. Oprian et al., The structural basis of agonist-induced activation in constitutively active rhodopsin. *Nature* **471**(7340), 656–660 (2011). <https://doi.org/10.1038/nature09795>
12. X.E. Zhou, K. Melcher, H.E. Xu, Structure and activation of rhodopsin. *Acta Pharmacol. Sin.* **33**(3), 291–299 (2012). <https://doi.org/10.1038/aps.2011.171>
13. M.R. Fleissner, M.D. Bridges, E.K. Brooks, D. Cascio, T. Kalai, K. Hideg et al., Structure and dynamics of a conformationally constrained nitroxide side chain and applications in EPR spectroscopy. *Proc. Natl. Acad. Sci. USA* **108**(39), 16241 (2011). <https://doi.org/10.1073/pnas.1111420108>
14. M.R. Fleissner, D. Cascio, W.L. Hubbell, Structural origin of weakly ordered nitroxide motion in spin-labeled proteins. *Protein Sci.* **18**(5), 893–908 (2009). <https://doi.org/10.1002/pro.96>
15. D.T. Warshaviak, L. Serbulea, K.N. Houk, W.L. Hubbell, Conformational analysis of a nitroxide side chain in an α -helix with density functional theory. *J. Phys. Chem. B* **115**(2), 397–405 (2011). <https://doi.org/10.1021/jp108871m>
16. G. Jeschke, Conformational dynamics and distribution of nitroxide spin labels. *Prog. Nucl. Magn. Reson. Spectrosc.* **72**, 42–60 (2013). <https://doi.org/10.1016/j.pnmrs.2013.03.001>
17. D. Sezer, J.H. Freed, B. Roux, Using Markov models to simulate electron spin resonance spectra from molecular dynamics trajectories. *J. Phys. Chem. B* **112**(35), 11014–11027 (2008). <https://doi.org/10.1021/jp801608v>
18. D. Sezer, J.H. Freed, B. Roux, Parametrization, molecular dynamics simulation, and calculation of electron spin resonance spectra of a nitroxide spin label on a polyaniline α -helix. *J. Phys. Chem. B* **112**(18), 5755–5767 (2008). <https://doi.org/10.1021/jp711375x>
19. E. Darian, P.M. Gannett, Application of molecular dynamics simulations to spin-labeled oligonucleotides. *J. Biomol. Struct. Dyn.* **22**(5), 579–593 (2005). <https://doi.org/10.1080/07391102.2005.10507028>
20. P. Cekan, S.T. Sigurdsson, Spin labeled nucleic acids for EPR spectroscopic study of DNA and RNA structure and function. *Collect. Symp. Ser.* **7**, 225–228 (2005). <https://doi.org/10.1135/css200507225>
21. Z. Liang, J.H. Freed, R.S. Keyes, A.M. Bobst, An electron spin resonance study of DNA dynamics using the slowly relaxing local structure model. *J. Phys. Chem. B* **104**(22), 5372–5381 (2000). <https://doi.org/10.1021/jp994219f>
22. E.J. Hustedt, J.J. Kirchner, A. Spaltenstein, P.B. Hopkins, B.H. Robinson, Monitoring DNA dynamics using spin-labels with different independent mobilities. *Biochemistry* **34**(13), 4369 (1995). <https://doi.org/10.1021/bi00013a028>
23. P.Z. Qin, K. Hideg, J. Feigon, W.L. Hubbell, Monitoring RNA base structure and dynamics using site-directed spin labeling. *Biochemistry* **42**(22), 6772–6783 (2003). <https://doi.org/10.1021/bi027222p>
24. W.L. Hubbell, C.J. Lopez, C. Altenbach, Z. Yang, Technological advances in site-directed spin labeling of proteins. *Curr. Opin. Struct. Biol.* **23**(5), 725–733 (2013). <https://doi.org/10.1016/j.sbi.2013.06.008>
25. D.E. Budil, CW-EPR spectral simulations: slow-motion regime. *Methods Enzymol.* **563**, 143–170 (2015). <https://doi.org/10.1016/bs.mie.2015.05.024>
26. K.V. Vasavada, D.J. Schneider, J.H. Freed, Calculation of ESR spectra and related Fokker–Planck forms by the use of the Lanczos algorithm. II. Criteria for truncation of basis sets and recursive steps utilizing conjugate gradients. *J. Chem. Phys.* **86**(2), 647 (1987). <https://doi.org/10.1063/1.452319>
27. D.J. Schneider, J.H. Freed, Calculating slow motional magnetic resonance spectra: a user's guide. *Biol. Magn. Reson.* **8**(Spin Labeling), 1–76 (1989). https://doi.org/10.1007/978-1-4613-0743-3_1
28. D.E. Budil, S. Lee, S. Saxena, J.H. Freed, Nonlinear-least-squares analysis of slow-motion EPR spectra in one and two dimensions using a modified Levenberg–Marquardt algorithm. *J. Magn. Reson. Ser. A* **120**(2), 155–189 (1996). <https://doi.org/10.1006/jmra.1996.0113>
29. S. Stoll, A. Schweiger, EasySpin, a comprehensive software package for spectral simulation and analysis in EPR. *J. Magn. Reson.* **178**(1), 42–55 (2006). <https://doi.org/10.1016/j.jmr.2005.08.013>
30. J. Lehner, S. Stoll, Modeling of motional EPR spectra using hindered Brownian rotational diffusion and the stochastic Liouville equation. *J. Chem. Phys.* **152**(9), 094103 (2020). <https://doi.org/10.1063/1.5139935>

31. S. Stoll, *Computational Modeling and Least-Squares Fitting of EPR Spectra* (Wiley, London, 2014), p.69
32. C. Altenbach, C.J. Lopez, K. Hideg, W.L. Hubbell, Exploring structure, dynamics, and topology of nitroxide spin-labeled proteins using continuous-wave electron paramagnetic resonance spectroscopy. *Methods Enzymol.* **564**, 59–100 (2015). <https://doi.org/10.1016/bs.mie.2015.08.006>
33. W.L. Hubbell, C. Altenbach, Site-directed spin labeling of membrane proteins. *Methods Physiol. Ser. 1*, 224 (1994)
34. Z. Yang, M.D. Bridges, C.J. Lopez, O.Y. Rogozhnikova, D.V. Trukhin, E.K. Brooks et al., A triarylmethyl spin label for long-range distance measurement at physiological temperatures using T1 relaxation enhancement. *J. Magn. Reson.* **269**, 50–54 (2016). <https://doi.org/10.1016/j.jmr.2016.05.006>
35. M. Yulikov, Spectroscopically orthogonal spin labels and distance measurements in biomolecules, in *Electron Paramagnetic Resonance*, vol. 24, ed. by V. Chechik, D.M. Murphy, B. Gilbert (The Royal Society of Chemistry, London, 2014)
36. T.F. Cunningham, M.R. Putterman, A. Desai, W.S. Horne, S. Saxena, The double-histidine Cu²⁺-binding motif: a highly rigid, site-specific spin probe for electron spin resonance distance measurements. *Angew. Chem. Int. Ed. Engl.* **54**(21), 6330–6334 (2015). <https://doi.org/10.1002/anie.201501968>
37. Z. Wu, A. Feintuch, A. Collauto, L.A. Adams, L. Aurelio, B. Graham et al., Selective distance measurements using triple spin labeling with Gd³⁺, Mn²⁺, and a nitroxide. *J. Phys. Chem. Lett.* **8**(21), 5277–5282 (2017). <https://doi.org/10.1021/acs.jpcclett.7b01739>
38. L. Columbus, T. Kalai, J. Jekoe, K. Hideg, W.L. Hubbell, Molecular motion of spin labeled side chains in α -helices: analysis by variation of side chain structure. *Biochemistry* **40**(13), 3828–3846 (2001). <https://doi.org/10.1021/bi002645h>
39. L. Columbus, W.L. Hubbell, A new spin on protein dynamics. *Trends Biochem. Sci.* **27**(6), 288–295 (2002). [https://doi.org/10.1016/s0968-0004\(02\)02095-9](https://doi.org/10.1016/s0968-0004(02)02095-9)
40. Z. Guo, D. Cascio, K. Hideg, T. Kalai, W.L. Hubbell, Structural determinants of nitroxide motion in spin-labeled proteins: tertiary contact and solvent-inaccessible sites in helix G of T4 lysozyme. *Protein Sci.* **16**(6), 1069–1086 (2007). <https://doi.org/10.1110/ps.062739107>
41. H.S. McHaourab, M.A. Lietzow, K. Hideg, W.L. Hubbell, Motion of spin-labeled side chains in T4 lysozyme. Correlation with protein structure and dynamics. *Biochemistry* **35**(24), 7692–7704 (1996). <https://doi.org/10.1021/bi960482k>
42. H.S. McHaourab, K.J. Oh, C.J. Fang, W.L. Hubbell, Conformation of T4 lysozyme in solution. Hinge-bending motion and the substrate-induced conformational transition studied by site-directed spin labeling. *Biochemistry* **36**(2), 307–316 (1997). <https://doi.org/10.1021/bi962114m>
43. H.S. McHaourab, T. Kalai, K. Hideg, W.L. Hubbell, Motion of spin-labeled side chains in T4 lysozyme: effect of side chain structure. *Biochemistry* **38**(10), 2947–2955 (1999). <https://doi.org/10.1021/bi9826310>
44. T. Kalai, J. Jekoe, W.L. Hubbell, K. Hideg, Synthesis of 2,2- and 2,5-disubstituted 1-oxyl pyrrolidine radicals as new homobifunctional cross-linking spin labels. *Synthesis* **13**, 2084–2088 (2003). <https://doi.org/10.1055/s-2003-41053>
45. T. Kalai, C.P. Sar, J. Jeko, K. Hideg, Synthesis of new pyrrolidine nitroxide epoxides as versatile paramagnetic building blocks. *Tetrahedron Lett.* **43**(45), 8125–8127 (2002). [https://doi.org/10.1016/s0040-4039\(02\)01911-1](https://doi.org/10.1016/s0040-4039(02)01911-1)
46. S. Gadanyi, T. Kalai, J. Jeko, Z. Berente, K. Hideg, Synthesis of 2-substituted pyrrolidine nitroxide radicals. *Synthesis* **14**, 2039–2046 (2000). <https://doi.org/10.1055/s-2000-8727>
47. C.P. Sar, J. Jeko, P. Fajer, K. Hideg, Synthesis and reactions of new alkynyl-substituted nitroxide radicals. *Synthesis* **6**, 1039–1045 (1999). <https://doi.org/10.1055/s-1999-3503>
48. R.M. Loesel, R. Philipp, T. Kalai, K. Hideg, W.E. Trommer, Synthesis and application of novel bifunctional spin labels. *Bioconjugate Chem.* **10**(4), 578–582 (1999). <https://doi.org/10.1021/bc980138v>
49. C.P. Sar, J. Jeko, K. Hideg, Synthesis of 3,4-disubstituted 2,5-dihydropyrrol-1-yloxyl spin label reagents. *Synthesis* **10**, 1497–1500 (1998). <https://doi.org/10.1055/s-1998-2177>
50. D. Toledo Warshaviak, V.V. Khramtsov, D. Cascio, C. Altenbach, W.L. Hubbell, Structure and dynamics of an imidazole nitroxide side chain with strongly hindered internal motion in proteins. *J. Magn. Reson.* **232**, 53–61 (2013). <https://doi.org/10.1016/j.jmr.2013.04.013>

51. N.L. Fawzi, M.R. Fleissner, N.J. Anthis, T. Kalai, K. Hideg, W.L. Hubbell et al., A rigid disulfide-linked nitroxide side chain simplifies the quantitative analysis of PRE data. *J. Biomol. NMR* **51**(1–2), 105–114 (2011). <https://doi.org/10.1007/s10858-011-9545-x>
52. M.R. Fleissner, E.M. Brustad, T. Kalai, C. Altenbach, D. Cascio, F.B. Peters et al., Site-directed spin labeling of a genetically encoded unnatural amino acid. *Proc. Natl. Acad. Sci. USA* **106**(51), 21637 (2009). <https://doi.org/10.1073/pnas.0912009106>
53. J.N. Ollivierre, D.E. Budil, P.J. Beuning, Electron spin labeling reveals the highly dynamic N-terminal arms of the SOS mutagenesis protein UmuD. *Mol. BioSyst.* **7**(12), 3183–3186 (2011). <https://doi.org/10.1039/c1mb05334e>
54. J. McCoy, W.L. Hubbell, High-pressure EPR reveals conformational equilibria and volumetric properties of spin-labeled proteins. *Proc. Natl. Acad. Sci. USA* **108**(4), 1331 (2011). <https://doi.org/10.1073/pnas.1017877108>
55. M.T. Lerch, J. Horwitz, J. McCoy, W.L. Hubbell, Circular dichroism and site-directed spin labeling reveal structural and dynamical features of high-pressure states of myoglobin. *Proc. Natl. Acad. Sci. USA* **110**(49), E4714–E4722 (2013). <https://doi.org/10.1073/pnas.1320124110>
56. J.H. Freed, G.K. Fraenkel, Alternating line widths and related phenomena in the electron spin resonance spectra of nitro-substituted benzene anions. *J. Chem. Phys.* **41**(3), 699–716 (1964). <https://doi.org/10.1063/1.1725949>
57. Z.T. Farahbakhsh, K. Hideg, W.L. Hubbell, Photoactivated conformational changes in rhodopsin: a time-resolved spin label study. *Science (Washington, DC, 1883–)* **262**(5138), 1416 (1993). <https://doi.org/10.1126/science.8248781>
58. Z.T. Farahbakhsh, K.D. Ridge, H.G. Khorana, W.L. Hubbell, Mapping light-dependent structural changes in the cytoplasmic loop connecting helices C and D in rhodopsin: a site-directed spin labeling study. *Biochemistry* **34**(27), 8812 (1995). <https://doi.org/10.1021/bi00027a033>
59. D.L. Farrens, C. Altenbach, K. Yang, W.L. Hubbell, H.G. Khorana, Requirement of rigid-body motion of transmembrane helices for light activation of rhodopsin. *Science (Washington, DC)* **274**(5288), 768–770 (1996). <https://doi.org/10.1126/science.274.5288.768>
60. J. Zhao, M. Elgeti, E.S. O'Brien, C.P. Sár, A.E. Daibani, J. Heng et al., Conformational dynamics of the μ -opioid receptor determine ligand intrinsic efficacy. *bioRxiv* (2023). <https://doi.org/10.1101/2023.04.28.538657>
61. N. Van Eps, C. Altenbach, L.N. Caro, N.R. Latorraca, S.A. Hollingsworth, R.O. Dror et al., Gi- and Gs-coupled GPCRs show different modes of G-protein binding. *Proc. Natl. Acad. Sci. USA* **115**(10), 2383–2388 (2018). <https://doi.org/10.1073/pnas.1721896115>
62. C.J. Lopez, Z. Yang, C. Altenbach, W.L. Hubbell, Conformational selection and adaptation to ligand binding in T4 lysozyme cavity mutants. *Proc. Natl. Acad. Sci. USA* **110**(46), E4306 (2013). <https://doi.org/10.1073/pnas.1318754110>
63. R.A. Strangeway, H.S. McHaourab, J.R. Luglio, W. Froncisz, J.S. Hyde, A general purpose multiquantum electron paramagnetic resonance spectrometer. *Rev. Sci. Instrum.* **66**(9), 4516–4528 (1995). <https://doi.org/10.1063/1.1146437>
64. G.R. Eaton, S.S. Eaton, Advances in rapid scan EPR spectroscopy. *Methods Enzymol.* **666**, 1–24 (2022). <https://doi.org/10.1016/bs.mie.2022.02.013>
65. G.L. Millhauser, J.H. Freed, Two-dimensional electron spin echo spectroscopy and slow motions. *J. Chem. Phys.* **81**(1), 37–48 (1984). <https://doi.org/10.1063/1.447316>
66. M.D. Bridges, Z. Yang, C. Altenbach, W.L. Hubbell, Analysis of saturation recovery amplitudes to characterize conformational exchange in spin-labeled proteins. *Appl. Magn. Reson.* **48**(11), 1315–1340 (2017). <https://doi.org/10.1007/s00723-017-0936-3>
67. J.S. Hwang, R.P. Mason, L.P. Hwang, J.H. Freed, Electron spin resonance studies of anisotropic rotational reorientation and slow tumbling in liquid and frozen media. III. Perdeuterated 2,2,6,6-tetramethyl-4-piperidone N-oxide and an analysis of fluctuating torques. *J. Phys. Chem.* **79**(5), 489–511 (1975). <https://doi.org/10.1021/j100572a017>
68. J.S. Hwang, K.V.S. Rao, J.H. Freed, An electron spin resonance study of the pressure dependence of ordering and spin relaxation in a liquid crystalline solvent. *J. Phys. Chem.* **80**(13), 1490 (1976). <https://doi.org/10.1021/j100554a019>
69. J.H. Freed, Nitroxides and chemical physics. *Kem. Kemi.* **9**(1), 50 (1982)
70. J.H. Freed, A. Nayeem, S.B. Rananavare, ESR and molecular motions in liquid crystals: motional narrowing. *NATO ASI Ser. Ser. C.* **431**, 271–312 (1994)
71. D. Xu, J.K. Moscicki, D.E. Budil, J.H. Freed, E. Hall, C.K. Ober, ESR studies of molecular dynamics of a liquid crystalline polyether. *Polym. Prepr. (Am. Chem. Soc. Div. Polym. Chem.)* **35**(1), 809 (1994)

72. M. Ge, D.E. Budil, J.H. Freed, An electron spin resonance study of interactions between phosphatidylcholine and phosphatidylserine in oriented membranes. *Biophys. J.* **66**(5), 1515 (1994). [https://doi.org/10.1016/s0006-3495\(94\)80942-7](https://doi.org/10.1016/s0006-3495(94)80942-7)
73. L.J. Libertini, C.A. Burke, P.C. Jost, O.H. Griffith, An orientation distribution model for interpreting ESR line shapes of ordered spin labels. *J. Magn. Reson.* (1969) **15**(3), 460–476 (1974). [https://doi.org/10.1016/0022-2364\(74\)90148-6](https://doi.org/10.1016/0022-2364(74)90148-6)
74. E. Meirovitch, A. Nayeem, J.H. Freed, Analysis of protein-lipid interactions based on model simulations of electron spin resonance spectra. *J. Phys. Chem.* **88**(16), 3454 (1984). <https://doi.org/10.1021/j150660a018>
75. K.A. Earle, D.E. Budil, Calculating slow-motion ESR spectra of spin-labeled polymers, in *Advanced ESR methods in polymer research*. ed. by S. Schlick (Wiley, New York, 2006)
76. D.E. Budil, K.L. Sale, K.A. Khairy, P.G. Fajer, Calculating slow-motional electron paramagnetic resonance spectra from molecular dynamics using a diffusion operator approach. *J. Phys. Chem. A* **110**(10), 3703–3713 (2006). <https://doi.org/10.1021/jp054738k>
77. K. Khairy, P. Fajer, D. Budil, Simulation of slow motion EPR spectra with a general hindering potential expanded in spherical harmonics. *Biophys. J.* **96**(3), 311a (2009). <https://doi.org/10.1016/j.bpj.2008.12.1550>
78. E.J. Hustedt, A.I. Smirnov, C.F. Laub, C.E. Cobb, A.H. Beth, Molecular distances from dipolar coupled spin-labels: the global analysis of multifrequency continuous wave electron paramagnetic resonance data. *Biophys. J.* **72**(4), 1861–1877 (1997). [https://doi.org/10.1016/s0006-3495\(97\)78832-5](https://doi.org/10.1016/s0006-3495(97)78832-5)
79. M.T. Lerch, Z. Yang, C. Altenbach, W.L. Hubbell, High-pressure EPR and site-directed spin labeling for mapping molecular flexibility in proteins. *Methods Enzymol.* **564**, 29–57 (2015). <https://doi.org/10.1016/bs.mie.2015.07.004>

Publisher's Note Springer Nature remains neutral with regard to jurisdictional claims in published maps and institutional affiliations.